Microfluid Nanofluid
DOI 10.1007/s10404-012-1000-0

RESEARCH PAPER

Surface–gas interaction effects on nanoscale gas flows

Murat Barisik · Ali Beskok

Received: 25 February 2012 / Accepted: 8 April 2012

Abstract Molecular dynamics (MD) method is used to simulate shear driven argon gas flows in the early transition and free molecular flow regimes to investigate surface effects as a function of the surface–gas potential strength ratio ($\varepsilon_{wf}/\varepsilon_{ff}$). Results show a bulk flow region and a near wall region that extends three molecular diameters away from the surfaces. Within the near wall region the velocity, density, and shear stress distributions exhibit deviations from the kinetic theory predictions. Increased $\varepsilon_{wf}/\varepsilon_{ff}$ results in increased gas density, leading toward monolayer adsorption on surfaces. The near wall velocity profile shows reduced gas slip, and eventually velocity stick with increased $\varepsilon_{wf}/\varepsilon_{ff}$. Using MD predicted shear stress values and kinetic theory, tangential momentum accommodation coefficients (TMAC) are calculated as a function of $\varepsilon_{wf}/\varepsilon_{ff}$, and TMAC values are shown to be independent of the Knudsen number. Presence of this near wall region breaks down the dynamic similarity between rarefied and nanoscale gas flows.

Keywords Wall force field effects · Tangential momentum accommodation coefficient · Shear stress · Rarefied gas flow

1 Introduction

With the advent of micro and nanotechnology, new sensors, resonators and scanning probes with sub-micron to nano meter size characteristic dimensions are being developed (Ekinci and Roukes 2008; Clelanda et al. 2002; Husain et al. 2003; Verbridge et al. 2008). In such small scales, surface forces dominate over body forces, and surface–fluid interactions play a key role in momentum and energy transport. Nanoscale device components working in air under room conditions experience flow regimes that are substantially different from the classical continuum approximation. For example, the tip of an atomic force microscope (AFM) experiences harmonic variations in probe-surface separation distance from sub-micron down to the nanometer scale. During its oscillatory motion, the surrounding thin layer of gas induces a damping force on the tip, which is comparable with the AFM force output (Zhang et al. 2009). The first step in proper modeling of flows in such small scales is the recognition of the rarefaction and nonequilibrium effects described by the local Knudsen number ($Kn = \lambda/H$, where λ is the local gas mean free path and H is the characteristic flow dimension). For $Kn \geq 10$, the flow is in the free molecular regime, where gas–wall collisions are dominant and the collisionless Boltzmann equation can be used. For $0.1 \leq Kn \leq 10$, the flow is in the transition regime, where gas–gas and gas–wall collisions become equally important. Mathematical modeling of these flows requires utilization of Boltzmann equation, or direct simulation Monte Carlo (DSMC). High-order continuum approximations such as the Burnett and Grad equations can also be used (Karniadakis et al. 2005). For the AFM example, one can analyze the squeeze film damping problem using the kinetic theory, which models gas–wall interactions via various scattering kernels or the tangential momentum accommodation coefficient, TMAC (α) (Guo and Alexeenko 2009; Bidkar et al. 2009; Gallis and Torczynski 2004). This classical approach mostly neglects the *surface force interactions between gas and*

M. Barisik · A. Beskok (✉)
Mechanical and Aerospace Engineering Department,
Institute of Micro and Nanotechnology,
Old Dominion University, Norfolk,
VA 23529-0247, USA
e-mail: abeskok@odu.edu

Published online: 30 May 2012

wall molecules. However, many molecular simulation and experimental studies in the literature reported significant effects of *surface–gas collisions* and *adsorbed gas molecules* on mechanical performance of micro- and nanoscale devices (Honig et al. 2010; Feng and Jiang 2011; Yang et al. 2011; Enguang 2002; Huang et al. 2008; Veijola et al. 1998; Gad-el-Hak 1999).

Rarefied gas flows can be characterized using the Reynolds (*Re*), Mach (*M*), and Knudsen (*Kn*) numbers. These three parameters are interdependent for ideal gas flows. Hence, matching two dimensionless groups, preferably the *Kn* and *M*, can maintain the dynamic similarity for rarefied gas flows (Beskok and Karniadakis 1994). However, nanoscale gas flows also experience *surface force field effects*. Hence, "dynamic similarity" of gas flows in low pressure environments (i.e., large λ) and nanoscale domains is questionable. Even for the most simplified case of atomically smooth noncharged surfaces, van der Waals force field interactions between the wall and gas molecules induce variations in momentum and energy transport within the wall force field penetration depth, which extends typically three molecular diameters ($\sim$1 nm) from each wall. As a result, 40 % of a 5-nm height channel would experience the wall force field effects, within which the transport could significantly deviate from the kinetic theory predictions. Inside the wall force penetration depth, solid surfaces induce body forces on fluid molecules, which result in surface-induced stresses. Stresses generated by the surface–particle interactions are identified as the "*surface virial*." Our earlier study was focused on stress variations in gas, dense gas and liquid argon confined in stationary nanochannels, where the "surface virial" created anisotropic normal stresses for dilute and dense gas phases in the near wall region (Barisik and Beskok 2011a). This is followed with the study of shear driven argon gas flows in nanochannels, where three dimensional MD simulations have shown deviations of density and velocity profiles in the near-wall region from the kinetic theory-based calculations (Barisik and Beskok 2011b). These deviations were found to be independent of the channel dimensions, base pressure and Knudsen number, and they were uniquely defined by the surface–gas potential strength ratio, which was fixed at $\varepsilon_{wf}/\varepsilon_{ff} = 1$. This work also outlined a methodology for calculation of TMAC values.

The tangential momentum accommodation coefficient was introduced by Maxwell as the fraction of gas molecules reflecting diffusively from a solid surface. TMAC value determines the tangential momentum exchange between gas and wall molecules, and it is heavily used in theoretical and numerical studies for rarefied, micro- and nanoscale gas flows. Several studies were conducted to determine its value using molecular beam and micro- and nanochannel gas flow experiments (Arkilic et al. 2001; Bentz et al. 1997, 2001; Goodman and Wachman 1976; Gronych et al. 2004; Rettner 1998; Sazhin et al. 2001), while the numerical research included MD simulations of single gas molecules interacting with crystalline surfaces (Arya et al. 2003; Chirita et al. 1993, 1997; Finger et al. 2007), two- and three-dimensional MD simulations (Cao et al. 2005; Sun and Li 2010, 2011), and coupled MD/DSMC models (Yamamato et al. 2006). Even though factors affecting the TMAC value are not well understood, these recent investigations demonstrated sensitivity of the accommodation coefficient to the surface–gas couple interaction parameters. In addition, gas adsorption on the surface is known to induce significant effects on transport (Zhou 2007; Lee and Aluru 2010; Finger et al. 2007; Sun and Li 2008).

The *objective* of this manuscript is to investigate nanoscale shear-driven gas flows as a function of the wall force field effects. To address this, we performed two different sets of molecular dynamics (MD) simulations at modified Knudsen number ($k = (\sqrt{\pi}/2)\,Kn$) values of $k = 1$ and $k = 10$, and for surface–gas pair interaction strength ratios of $1 \leq \varepsilon_{wf}/\varepsilon_{ff} \leq 6$. The range of simulation parameters covers the early transition and free molecular flow regimes, which are typical of nanoscale gas flows under standard conditions, and subjected to weak to strong gas–surface interactions. This work is organized as follows: In Sect. 2, we describe MD simulation parameters, explain the stress tensor computations and methods utilized in the MD algorithm. In Sect. 3, we present gas flow results at $k = 1$ and $k = 10$. Comparisons are made on density, velocity and shear stress profiles for each case. MD predictions of shear stress and velocity profiles are compared with the kinetic theory calculations, and TMAC values are predicted. Finally, Sect. 4 presents the conclusions.

2 Three-dimensional MD simulation details

Shear-driven argon gas flows at $k = 1$ and $k = 10$ are simulated between two parallel plates separated with a distance h. Thermodynamic state of argon was fixed at 298 K and 113.4 kPa, corresponding to 1.896 kg/m^3 density and 54 nm mean free path (λ). Channel heights of $h = 54$ and $h = 5.4$ nm are used to establish $k = 1$ and $k = 10$ flows, respectively. Periodic boundary conditions are applied in the stream wise and lateral directions. Since gas flows evolve through intermolecular collisions, simulation domains span one mean free path in the periodic directions. Using such large domains in MD can be computationally overwhelming due to the excessively large number of wall molecules. We addressed this computational difficulty using the recently developed Smart Wall Molecular Dynamics (SWMD) algorithm, which reduces

the memory requirements for modeling surfaces. For the three-dimensional FCC crystal structured wall with 0.54 nm cube side length and (100) plane facing the gas molecules (used here), the SWMD limits memory use of a semi-infinite wall slab into a stencil of 74 wall molecules (Barisik et al. 2010). The current SWMD is a fixed lattice model, where the wall molecules are rigid and keep their corresponding FCC positions (i.e., cold wall model). When a gas molecule approaches the surface and enters the near wall region, the SWMD wall stencil appears to model the wall. Figure 1 schematically shows this procedure, where patchy walls on the right figure show SWMD stencils during a simulation. Although there are many wall stencils at a given instant, all of these are modeled using the same 74 wall molecules shown in the middle figure, resulting in significant computational advantages (Barisik et al. 2010).

Shear-driven flow is obtained by moving the top and bottom channel walls in opposite directions with a characteristic velocity of $U_w = M\sqrt{\gamma k_b T/m}$, where M is the Mach number, γ is the adiabatic index (5/3 for monatomic molecules), k_b is the Boltzmann constant (1.3806×10^{-23} J K^{-1}), T (298 K) is the temperature, and m is the mass of gas molecules. Mass for an argon molecule is $m = 6.63 \times 10^{-26}$ kg, its molecular diameter is $\sigma = 0.3405$ nm and the depth of the potential well for argon is $\varepsilon = 119.8 \times k_b$. The latter parameter defines the gas–gas interaction strength, and it is identified as ε_{ff}. For simplicity, the walls have molecular mass and diameter equivalent to argon ($m_{\text{wall}} = m_{\text{Ar}}$, $\sigma_{\text{wall}} = \sigma_{\text{Ar}}$).

Lenard–Jones (L–J) 6–12 potential is utilized to model the van der Waals interactions between gas–gas and gas–wall molecules. The ratio of the potential strength for gas–wall interactions (ε_{wf}) to the gas–gas molecular interactions (ε_{ff}) is assigned to have values of $\varepsilon_{\text{wf}}/\varepsilon_{\text{ff}} = 1$, 2, 3, 4, 5 and 6. Since the L–J potential vanishes at larger molecular distances, only the interactions with particles within a certain cut-off radius (r_c) are calculated. Therefore, the intermolecular interaction forces are truncated and switched to zero at a certain cut-off distance (Allen and Tildesley 1989). The truncated (6–12) Lennard–Jones (L–J) potential is given as

$$V_{truncated}(r_{ij}) = 4\varepsilon\left(\left(\left(\frac{\sigma}{r_{ij}}\right)^{12} - \left(\frac{\sigma}{r_{ij}}\right)^{6}\right) - \left(\left(\frac{\sigma}{r_c}\right)^{12} - \left(\frac{\sigma}{r_c}\right)^{6}\right)\right), \quad (1)$$

where r_{ij} is the intermolecular distance, ε is the depth of the potential well, σ is the molecular diameter and r_c is the cut-off radius. In this study we utilize $r_c = 1.08$ nm, which is approximately equal to 3.17σ for argon molecules. At this cut-off-distance the attractive part of the LJ potential is reduced to 0.00392ε. Our algorithm utilizes the well-known link cell method to handle particle–particle interactions (Allen and Tildesley 1989).

Simulations start from the Maxwell–Boltzmann velocity distribution for gas molecules at 298 K. Initial particle distribution is evolved 10^6 time steps (4 ns) to reach an isothermal steady state using 4 fs ($\sim 0.002\tau$) time steps, after which, 2×10^6 time steps (8 ns) are performed for time averaging. Longer time averaging has also been performed to confirm the convergence of density, stress and velocity profiles to steady state. To capture the property variations within the near wall region accurately and with same resolution, all simulation domains are divided into equally sized slab bins of 0.054 nm in the wall normal direction. As a result, $k = 1$ cases use 1,000 slab bins, while $k = 10$ case utilizes 100 slab bins. Canonical ensemble (NVT, i.e., constant mole, N, volume, V, and temperature, T) is performed by utilizing a thermostat. We employed the Nose–Hoover algorithm (Evans and Hoover 1986) as a global thermostat inside the local sub-domains to obtain isothermal condition of 298 K with a relaxation time of ~ 0.2 ps. Sub-domains have 0.54 nm heights through the entire span which is 10 times larger than the utilized bin size.

Irving–Kirkwood (I–K) expression is utilized to compute the stress tensor components for an N particle system with unity differential operator approximation as follows (Irving and Kirkwood 1950; Todd et al. 1995),

$$S_{kl} = \frac{1}{\text{Vol}}\left\langle \sum_{i}^{N} m^i (V_k^i - \bar{V}_k^i)(V_i^i - \bar{V}_i^i) + W_{kl} \right\rangle, \quad (2)$$

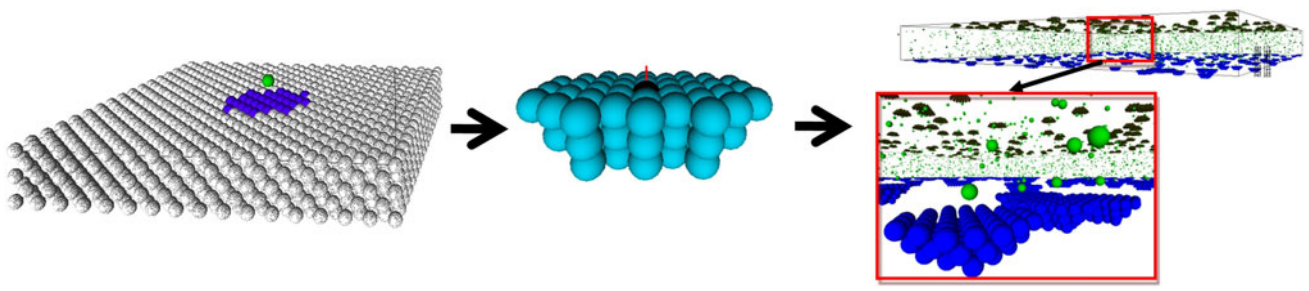

Fig. 1 Illustration of the SWMD procedure

$$W_{kl} = \frac{1}{2}\sum_{i,j}^{N}(r_k^j - r_k^i)f_l^{i,j}, \tag{3}$$

where the first term on the right hand side of Eq. (2) is the kinetic, and the W_{kl} term is the virial component. In the kinetic part, m^i is the atomic mass of particle i, while k and l are the axes of the Cartesian coordinate system, V_k^i and V_l^i are the peculiar velocity components of particle i in the k and l directions, and $\bar{V}_k^i$ and $\bar{V}_l^i$ are the local average streaming velocities at the position of particle i, in the k and l directions, respectively. The local streaming velocities within each bin were initially calculated and subtracted from the local molecular velocities. For the virial component, $(r_k^j - r_k^i)$ in Eq. (3) is the *kth* component of the relative distance vector between particles i and j, and $f_l^{i,j}$ is the *lth* component of the intermolecular force exerted on particle i by particle j. Virial of each molecule is calculated according to its interactions with the other molecules that are one cut-of-distance away using Eq. (3) in the link cell algorithm. After which, Eq. (2) is applied inside each averaging bin for each time step.

Computations of the stress tensor for an atomistic system have two additive components. The first term in the Irving–Kirkwood expression is the kinetic contribution from throughput of linear momentum resulting from the particle velocities and it captures the ideal gas law regardless of the fluid's state. The second component is the virial term, which is an internal contribution from intermolecular forces between the particles. Specifically, the virial part shown in Eq. (3) has two additive components originating from particle–particle and surface–particle interactions. For a domain free of solid boundaries, particle–particle virial acts as a correction to the ideal gas law by taking account the particle interactions. Thus, molecular dynamics can estimate the correct thermodynamic state in various density domains by calculating the particle–particle virial terms using a sufficiently large intermolecular interaction cut-off distance. For a detailed investigation of normal stress calculations for gas, dense gas and liquid domains, the readers are referred to (Barisik and Beskok 2011a). Surface force field effects on the stress distribution are calculated using the surface–particle virial, which has significant contributions to all components of the stress tensor within the wall force field penetration region.

3 Results

In this section, results of Argon gas confined in nanochannels are presented in two different sets. Initially, shear-driven gas flows in the early transition regime ($k = 1$) are simulated in 54 nm height channels. This is followed with gas flows confined in 5.4 nm height channels ($k = 10$), corresponding to the free molecular flow regime. In both cases, we studied surface effects at different $\varepsilon_{wf}/\varepsilon_{ff}$ ratios that vary between 1 and 6.

3.1 Gas flows at $k = 1$

We start our investigations with argon gas confined in 54 nm height channel with different $\varepsilon_{wf}/\varepsilon_{ff}$ values. Snapshots of the simulation domains are shown in Fig. 2, where the gas molecules are shown in green. Presence of a gas molecule within the wall force penetration region requires utilization of the smart wall stencil on the surface, which are shown in blue and black on the bottom and top surfaces of the channel, respectively. Increase in the surface–gas interaction strength results in more gas molecules in the vicinity of the surface. The $\varepsilon_{wf}/\varepsilon_{ff} = 6$ case approaches to complete surface coverage, as can be seen in Fig. 2g. Since different $\varepsilon_{wf}/\varepsilon_{ff}$ values result in different number of adsorbed molecules on the surfaces, we start each simulation using the proper number of molecules to obtain the desired gas density in the bulk of the channels. Simulation details, such as the number of molecules used in computation of different $\varepsilon_{wf}/\varepsilon_{ff}$ ratio flows and the corresponding bulk density of argon are shown in Table 1.

Density distributions within 2 nm from the top wall are shown in Fig. 3a for each $\varepsilon_{wf}/\varepsilon_{ff}$ case. The wall is defined at the center of the first row of wall molecules facing the fluid. Therefore, gas molecules cannot penetrate to several bins neighboring the wall, and the gas density goes to zero within 0.2 nm from the walls. With the exception of the near wall regions, argon density is approximately 1.89 kg/m^3. Surface forces induce increased particle residence time inside the force penetration depth, which results in density buildup. For $\varepsilon_{wf}/\varepsilon_{ff} \leq 5$, there is a single density peak point near the surface. But at $\varepsilon_{wf}/\varepsilon_{ff} = 6$, we observe a second density peak which is much weaker than the first value (<0.3 % of the first peak value). It should be noted that this behavior is different than the dense gas case, where the second density peak value was comparable with the first one (48 % of first peak value) and indicated an onset of density layering due to the differences in the gas–gas virial effects as a result of increased bulk density (Barisik and Beskok 2011a). For the case of $\varepsilon_{wf}/\varepsilon_{ff} = 1$ density starts to deviate from its bulk value around 2.5σ from the wall, while the density profiles for $\varepsilon_{wf}/\varepsilon_{ff} = 6$ case penetrate approximately 3σ from the wall. This shows that increased $\varepsilon_{wf}/\varepsilon_{ff}$ values enhance the surface influence zone. For all cases, the near wall gas density increases with increasing the $\varepsilon_{wf}/\varepsilon_{ff}$, which is due to the adsorption of a single layer of argon gas molecules on the surface as can be seen in Fig. 2e–g. To categorize the adsorption behavior, we calculated the number of the gas molecules near the surface.

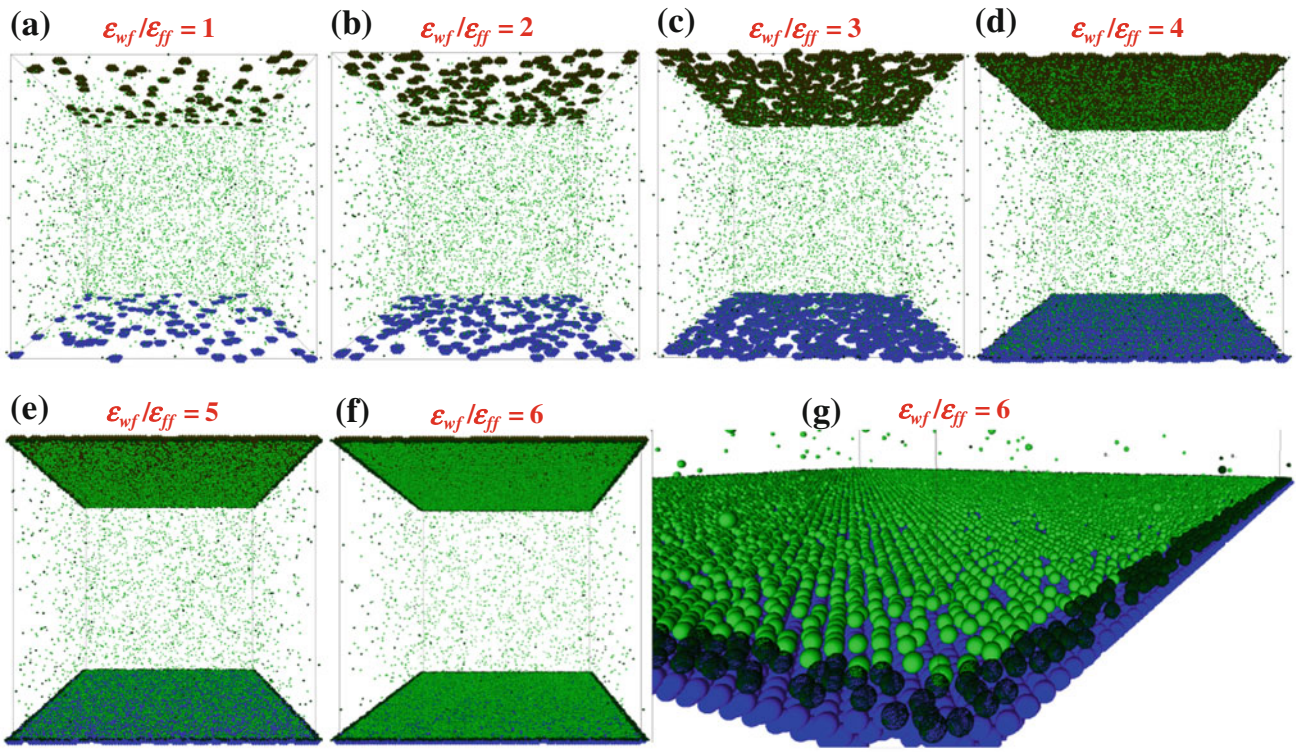

Fig. 2 Snapshots of argon gas flows at $k = 1$ with various $\varepsilon_{wf}/\varepsilon_{ff}$ values (**a**–**f**). All simulations are confined in 54 × 54 × 54 nm domains at 298 K and 113.4 kPa. **g** Shows adsorbed argon gas layer on the bottom surface for the $\varepsilon_{wf}/\varepsilon_{ff} = 6$ case

Table 1 Simulation details of $k = 1$ flows confined in 54-nm height channels at 298 K and 113.4 kPa

Theoretical free molecular shear stresses (τ_∞), corrected stress values for $k = 1$ flow ($\tau_{k=1}$), MD results (τ_{MD}) and TMAC predictions are tabulated for various $\varepsilon_{wf}/\varepsilon_{ff}$ values

$\varepsilon_{wf}/\varepsilon_{ff}$	No. of molecules	ρ_{bulk} (kg/m^3)	k	τ_∞ (kPa)	$\tau_{k=1}$ (kPa)	τ_{MD} (kPa)	TMAC
1	4,500	1.89	1.01	−23.97	−15.70	−9.51	0.75
2	4,700	1.87	1.02	−23.78	−15.62	−12.85	0.90
3	5,500	1.84	1.03	−23.42	−15.45	−13.77	0.94
4	10,000	1.90	1.00	−24.15	−15.66	−14.61	0.96
5	22,000	1.88	1.01	−23.89	−15.50	−15.02	0.98
6	36,000	1.85	1.03	−23.51	−15.25	−15.03	0.99

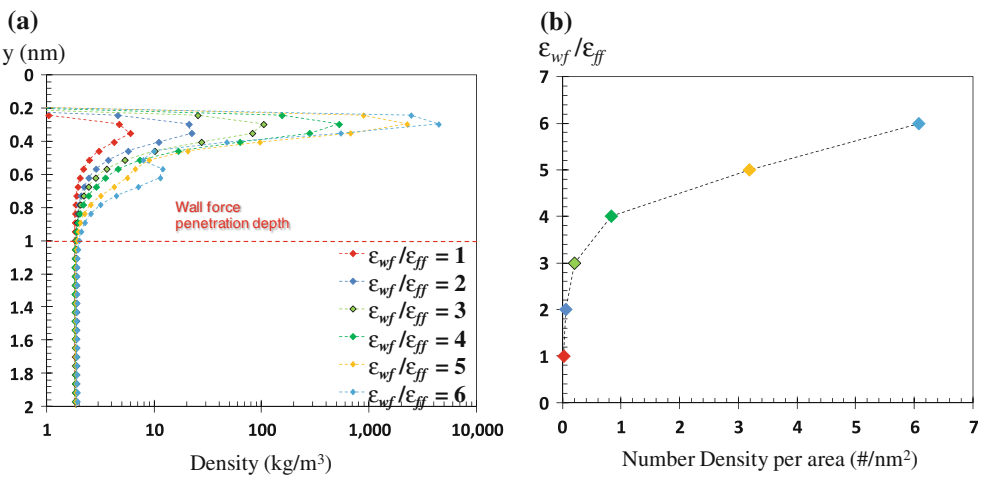

Fig. 3 Argon density variation in $k = 1$ flows within 2 nm from the wall for various $\varepsilon_{wf}/\varepsilon_{ff}$ values (**a**). Number density of argon molecules per surface area as a function of $\varepsilon_{wf}/\varepsilon_{ff}$ ratio (**b**)

Assuming a monolayer of adsorbate on surface, we consider the gas molecules σ away from the surface. For the current case, wall molecules penetrate 0.5σ into the simulation domain (since $y = 0$ is located at the center of wall molecules), therefore we calculate the sum of the gas molecules 1.5σ away from the surface. Figure 3b shows the number of molecules per unit surface area, which increases with increased $\varepsilon_{wf}/\varepsilon_{ff}$, and approaches to the maximum limit of single layer adsorption. For the $\varepsilon_{wf}/\varepsilon_{ff} = 6$ case, surface molecular coverage reaches 6.08 #/nm^2, while the hypothetical value for complete surface coverage due to the adsorption sites on a (1 0 0) surface is 6.86 #/nm^2.

Velocity profiles in half of the channel and the linearized Boltzmann (LB) solution for $k = 1$ flow subjected to the TMAC (α) values of $\alpha = 1$ and $\alpha = 0.75$ are shown in Fig. 4a. The MD velocity profiles agree with the kinetic theory predictions adopted from (Sone et al. 1990) in the bulk region. We observe a better match between the MD results for $\varepsilon_{wf}/\varepsilon_{ff} = 1$ case and the LB solution using $\alpha = 0.75$. Increase in $\varepsilon_{wf}/\varepsilon_{ff}$ increases the bulk velocity, which reaches to the LB solution of $\alpha = 1$ for $\varepsilon_{wf}/\varepsilon_{ff} \geq 3$ cases. MD velocity profiles show sudden changes within the force penetration depth. Since these deviations are confined in the 3σ region, their influence extends only 4 % of the domain for 54 nm height channel. Figure 4b shows zoomed view of this region to explore the velocity variation inside the wall force penetration depth. For $\varepsilon_{wf}/\varepsilon_{ff} \geq 3$, gas velocity reaches the wall velocity due to the adsorption of gas molecules on to the surface. Despite the large amount of slip velocity predicted by the kinetic theory solution, the near wall velocity profiles for $\varepsilon_{wf}/\varepsilon_{ff} \geq 3$ cases show velocity stick in $k = 1$ flows. This behavior is due to the wall force field that diminishes approximately 3σ away from the wall surface, after which the kinetic theory solution is valid.

Based on the kinetic theory of gases, shear stress for a shear driven flow in the free molecular flow regime ($Kn \rightarrow \infty$) can be written as (Fukui et al. 2005),

$$\tau_\infty = -\frac{\alpha}{2-\alpha}\rho U\sqrt{\frac{RT_w}{2\pi}} \tag{4}$$

where T_w is the wall temperature. The TMAC value can be interpreted as α portion of molecules reflecting diffusively, while $1-\alpha$ is the portion of molecules reflecting specularly. Specular reflections ($\alpha = 0$) will not drive the fluid, and result in zero shear stress. Therefore the shear stress for free molecular flows varies between a maximum value for $\alpha = 1$ to zero for $\alpha = 0$ based on Eq. (4). To consider the finite Knudsen number effects, we utilize

$$\frac{\tau}{\tau_\infty} = \frac{0.5297Kn^2 + 1.206Kn}{0.5297Kn^2 + 1.6277Kn + 0.603} \tag{5}$$

which is developed using numerical results from DSMC and solutions of the linearized Boltzmann equation. This relation is asymptotically consistent for free molecular and slip flow regimes, and accurately fit the data in the transition flow regime (Bahukudumbi et al. 2003). Theoretical free molecular shear stresses (τ_∞) and corrected stress values for $k = 1$ flow ($\tau_{k=1}$) are calculated for each simulation case by considering the gas bulk density. Results are tabulated in Table 1.

Figure 5 shows MD shear stress distribution in nanochannels within 1.2 nm distance from the top wall for each $\varepsilon_{wf}/\varepsilon_{ff}$ case. Despite the constant wall velocity of 64 m/s ($M = 0.2$) applied for each case, increase of $\varepsilon_{wf}/\varepsilon_{ff}$ increases the shear rates and shear stresses inside the channels. All $\varepsilon_{wf}/\varepsilon_{ff}$ cases are eventually at the same bulk density and k with slight fluctuations (Table 1). To make a fair comparison, we normalized the shear stress profiles using theoretical values corresponding to $k = 1$ and $\alpha = 1$ (shown by $\tau_{k=1}$) in Table 1. Dimensional values of MD shear stress results in the bulk region (τ_{MD}) are also tabulated. As can be seen in Fig. 5, shear stress is constant in the bulk region while the surface forces induce variations near the walls. This is due to the virial contribution of shear

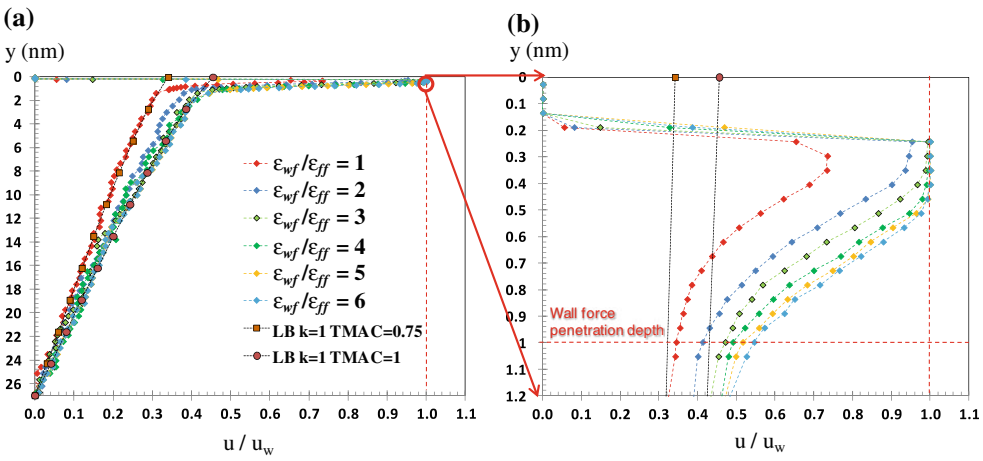

Fig. 4 Velocity profiles for $k = 1$ flows with different $\varepsilon_{wf}/\varepsilon_{ff}$ values in the half of the 54-nm height channel (**a**) and within 1.2 nm distance from the walls (**b**). Velocity profiles are normalized with the constant wall velocity of 64 m/s

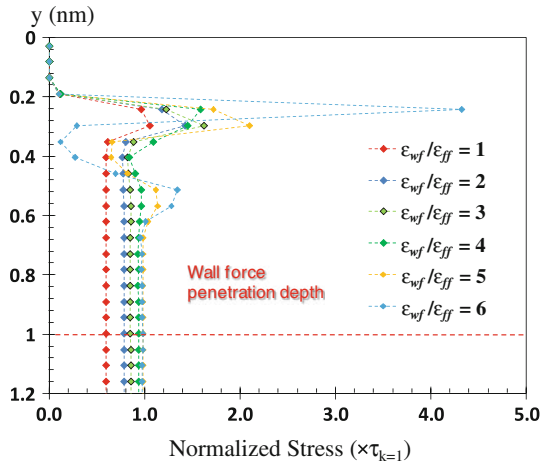

Fig. 5 Normalized shear stress distribution for various $\varepsilon_{wf}/\varepsilon_{ff}$ gas flows at $k = 1$. Normalization is obtained using the corresponding theoretical shear stress values for $k = 1$ and $\alpha = 1$ ($\tau_{k=1}$ in Table 1)

stress which is mostly negligible through the gas domains. In presence of a surface, the surface–gas virial and later the gas–gas virial of adsorbed molecules become dominant inside the force penetration depth. For $\varepsilon_{wf}/\varepsilon_{ff} \leq 3$, shear stress starts to deviate from its bulk value with a single peak point approximately σ distance from the wall. This peak induced by the surface virial decays closer to the surface due to the diminishing density at $y \approx 0.2$ nm. Interestingly, density and density-related properties are in decreasing trend while the surface virial peaks. This region, from one sigma distance to zero density, is the main location where wall and gas molecules interact with strong repulsive forces. An increase in the ε_{wf} value results in stronger surface–gas interactions; and hence, the surface virial becomes more dominant and increases the peak value. However, further increase of $\varepsilon_{wf}/\varepsilon_{ff}$ results in adsorption of gas molecules, and increases the importance of gas–gas virial terms. Starting with the $\varepsilon_{wf}/\varepsilon_{ff} = 4$ case, attractive interactions between the gas molecules near surface create a dip in the shear stress at the location of the first density peak. This is followed by a second shear stress peak point due to the repulsion between the molecules of first and second density peaks approximately 0.5 nm from the surface.

Comparing MD shear stress results with the theoretical values calculated using Eq. (4) and corrected for corresponding k value using Eq. (5), we predicted the TMAC values for argon gas interacting with different $\varepsilon_{wf}/\varepsilon_{ff}$ surfaces. Results in Table 1 show TMAC values varying from $\alpha = 0.75$ to $\alpha = 0.90$ for $1 \leq \varepsilon_{wf}/\varepsilon_{ff} \leq 6$. Since we predict the TMAC values directly using the bulk flow shear stress, it is important to verify the consistency of our TMAC predictions by comparing the velocity profiles obtained from MD simulations with the kinetic theory predictions for $k = 1$ flows at different TMAC values. Figure 6 shows the velocity profiles for $\varepsilon_{wf}/\varepsilon_{ff} = 1$ and $\varepsilon_{wf}/\varepsilon_{ff} = 2$ cases, which are in good agreement with the linearized Boltzmann solution using TMAC values of $\alpha = 0.75$ and $\alpha = 0.90$, respectively.

3.2 Gas flows at $k = 10$

Shear-driven gas flows at $k = 10$ inside 5.4 nm height channels are studied for various $\varepsilon_{wf}/\varepsilon_{ff}$ values. Simulation details are given in Table 2. Similar to the earlier case, adsorption of gas molecules on solid surfaces increases with increased $\varepsilon_{wf}/\varepsilon_{ff}$ values. Figure 7a shows density variations in half of the channel for different $\varepsilon_{wf}/\varepsilon_{ff}$ cases. Bulk density is constant while the surface forces result in density accumulation appearing as a single density peak inside the wall force penetration depth. The figure also presents the density profiles for $k = 10$ cases for comparison purposes. Identical density profiles are observed between different k flows at same $\varepsilon_{wf}/\varepsilon_{ff}$ values. In our earlier study, a universal behavior inside the wall force penetration depth of various $\varepsilon_{wf}/\varepsilon_{ff} = 1$ gas flows was

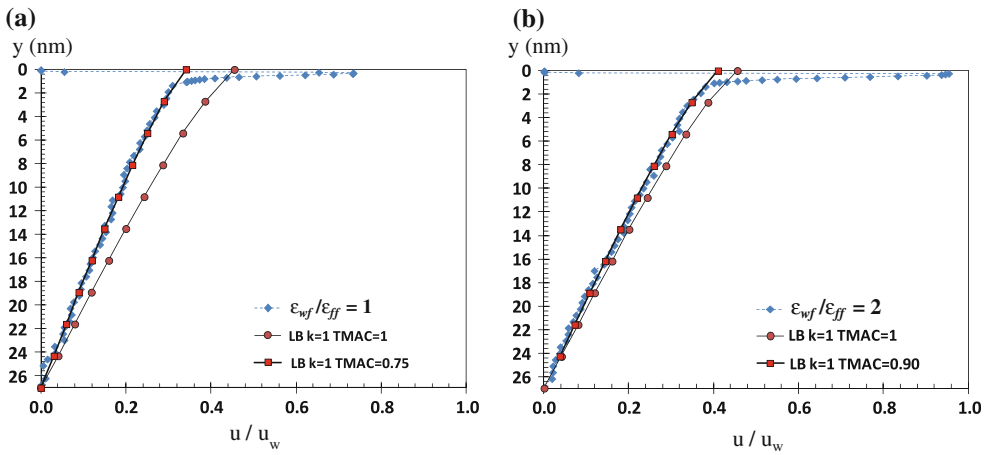

Fig. 6 Comparison of the velocity profiles for $k = 1$ flows in half of the 54-nm height channel with linearized Boltzmann solutions using $\alpha = 0.75$ for $\varepsilon_{wf}/\varepsilon_{ff} = 1$ (**a**) and $\alpha = 0.9$ for $\varepsilon_{wf}/\varepsilon_{ff} = 2$ (**b**)

Table 2 Simulation details of $k = 10$ flows within 5.4-nm height channels at 298 K and 113.4 kPa

Theoretical free molecular shear stresses (τ_∞), corrected stress values for $k = 1$ and $\alpha = 1$ flow ($\tau_{k=1}$), MD results (τ_{MD}) and TMAC predictions are tabulated for various $\varepsilon_{wf}/\varepsilon_{ff}$ values

$\varepsilon_{wf}/\varepsilon_{ff}$	No. of molecules	ρ_{bulk} (kg/m^3)	k	τ_∞ (kPa)	$\tau_{k=10}$ (kPa)	τ_{MD} (kPa)	TMAC
1	450	1.82	10.5	−23.12	−21.75	−13.07	0.75
2	690	1.88	10.1	−23.88	−22.42	−17.65	0.90
3	1,570	1.84	10.3	−23.39	−21.98	−18.83	0.93
4	5,300	1.77	10.7	−22.56	−21.24	−19.80	0.96
5	19,000	1.77	10.7	−22.39	−21.09	−20.26	0.98
6	32,000	1.99	9.6	−25.29	−23.65	−23.08	0.99

presented for the different values of the characteristic dimensions of confinement, gas density and k values (Barisik and Beskok 2011b). Results in Fig. 7a, further validate our previous findings by providing a universal density distribution for various $\varepsilon_{wf}/\varepsilon_{ff}$ values regardless of the Knudsen number.

In Fig. 7b, velocity profiles normalized with the wall velocity are plotted in half of the channel. In the bulk region, MD results agree with the linearized Boltzmann solutions with corresponding α values. Large velocity variations are observed within the force penetration depth, which covers 40 % of the simulation domain. Similar with the $k = 1$ cases, gas velocity reaches to the wall velocity for $\varepsilon_{wf}/\varepsilon_{ff} \geq 3$. At this point, one can specify location of the wall and the corresponding velocity boundary condition predicted by the current atomistic model. Due to the finite size of molecules and wall corrugation effects, gas molecules cannot penetrate closer than $y \approx 0.2$ nm. Depending on $\varepsilon_{wf}/\varepsilon_{ff}$, the maxima in gas density is at $0.3 \leq y \leq 0.34$ nm, while the shear stresses and gas velocities peak at $0.24 \leq y \leq 0.3$ nm. Observation of the velocity profiles clearly show location of the wall (from continuum point of view) around $y = 0.24$ nm. Using this information, we can conclude that $\varepsilon_{wf}/\varepsilon_{ff} \geq 3$ results in velocity stick boundary condition, while velocity slip is observed for lower $\varepsilon_{wf}/\varepsilon_{ff}$ values. This is a drastic difference from the LB solution, which indicates substantial velocity slip on the walls.

Shear stress variation in 5.4 nm height channel shows similar behavior with the earlier case of the $k = 1$, except that the bulk flow stress values are higher due to higher k (Table 2). Shear stress is constant in the bulk flow region, while the surface–gas interactions and for $\varepsilon_{wf}/\varepsilon_{ff} \geq 2$ the gas–gas interactions induce deviations in the wall force penetration depth. Using the same approach for $k = 1$ flow, we calculated the TMAC values of $k = 10$ flows for various $\varepsilon_{wf}/\varepsilon_{ff}$ cases, and tabulated them in Table 2. Starting with the value of 0.75 for $\varepsilon_{wf}/\varepsilon_{ff} = 1$, TMAC increases with increased ε_{wf}, and approaches unity for $\varepsilon_{wf}/\varepsilon_{ff} \geq 3$. TMAC variations for $k = 1$ and $k = 10$ flows for the studied cases are plotted in Fig. 8. TMAC variations as a function of $\varepsilon_{wf}/\varepsilon_{ff}$ are shown to be independent of the Knudsen number, which was also a conclusion we derived in an earlier study obtained for $\varepsilon_{wf}/\varepsilon_{ff} = 1$ flow at different k values (Barisik and Beskok 2011b).

4 Conclusions

Our findings show that surface–gas interaction strength uniquely defines the tangential momentum exchange between gas and wall molecules (i.e. TMAC) regardless of the local *Kn* value and channel dimensions. As a result, the bulk flow velocity profile, and shear stress are functions of the $\varepsilon_{wf}/\varepsilon_{ff}$ ratio and the Knudsen number. Kinetic

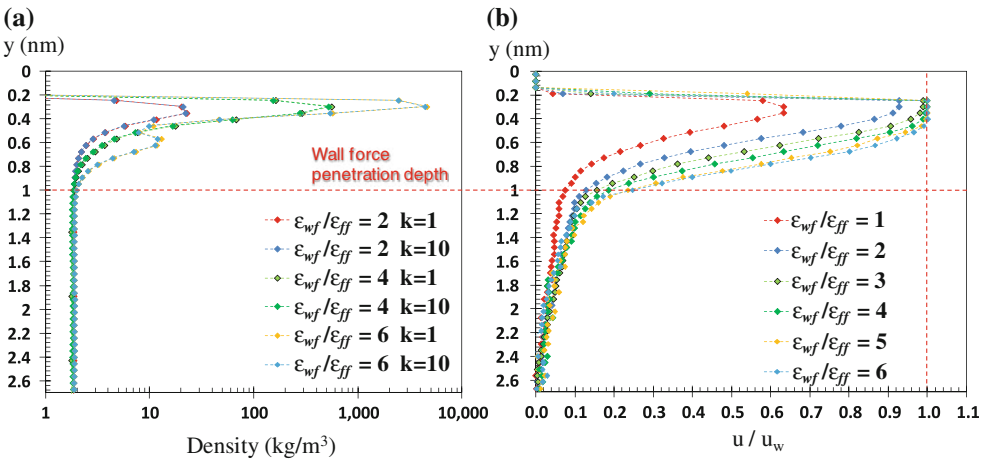

Fig. 7 Comparison of density profiles for $k = 1$ and $k = 10$ flows for $\varepsilon_{wf}/\varepsilon_{ff} = 2$, 4, and 6 within 2.7 nm distance from wall (**a**). Velocity profiles of $k = 10$ flows with different $\varepsilon_{wf}/\varepsilon_{ff}$ values in the half of the 5.4-nm height channel (**b**). Wall velocity is equal to 64 m/s

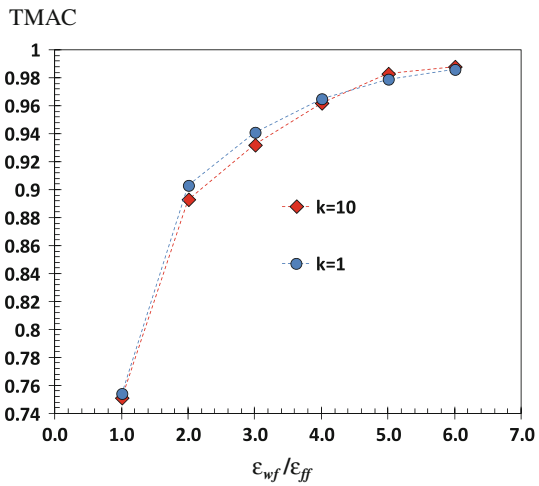

Fig. 8 TMAC variation of $k = 1$ and $k = 10$ flows as a function of the normalized gas–wall potential strength ratio $\varepsilon_{wf}/\varepsilon_{ff}$

theory-based velocity profiles using calculated TMAC values agree well with MD velocity profiles in the bulk flow region. Despite this agreement, MD results show formation of a near-wall region within three molecular diameters away from the surface. In this region, gas density and velocity increase with increased $\varepsilon_{wf}/\varepsilon_{ff}$ ratio. Although $\varepsilon_{wf}/\varepsilon_{ff} \geq 3$ cases result in velocity stick on the surface, induced by the density buildup and onset of adsorption, neglecting of this near-wall region results in slip of the bulk flow region, consistent with the kinetic theory predictions. Presence of this near wall region shows breakdown of the dynamic similarity between rarefied and nanoscale gas flows based on the Knudsen and Mach numbers. Hence, one should define a new dimensionless parameter as the ratio of the force field penetration depth to the characteristic channel dimension, where wall effects cannot be neglected for large values of this parameter. A good example of this is the $k = 10$ case obtained in 5.4 nm height channel, where the deviations from kinetic theory predictions extends over 40 % of the channel. Future work will focus on obtaining quantitative results for specified surface–gas couples (i.e., silicon–argon, etc) employing thermally interactive wall models.

Acknowledgments This work was supported by the National Science Foundation under Grant No. DMS 0807983.

References

Allen MP, Tildesley DJ (1989) Computer simulation of liquids. Oxford Science Publications Oxford University Press, New York

Arkilic EB, Breuer KS, Schmidt MA (2001) Mass flow and tangential momentum accommodation in silicon micromachined channels. J Fluid Mech 437:29–43

Arya G, Chang HC, Maginn EJ (2003) Molecular simulations of Knudsen wall-slip: effect of wall morphology. Mol Simul 29(10–11):697–709

Bahukudumbi P, Park JH, Beskok A (2003) A unified engineering model for steady and quasi-steady shear-driven gas microflows. Microscale Thermophys Eng 7:291–315

Barisik M, Beskok A (2011a) Equilibrium molecular dynamics studies on nanoscale confined fluids. Microfluid Nanofluid. doi:10.1007/s10404-011-0794-5

Barisik M, Beskok A (2011b) Molecular dynamics simulations of shear-driven gas flows in nano-channels. Microfluid Nanofluid. doi:10.1007/s10404-011-0827-0

Barisik M, Kim B, Beskok A (2010) Smart wall model for molecular dynamics simulations of nanoscale gas flows. Commun Comput Phys. doi:10.4208/cicp.2009.09.118

Bentz JA, Tompson RV, Loyalka SK (1997) The spinning rotor gauge: measurements of viscosity, velocity slip coefficients, and tangential momentum accommodation coefficients for N_2 and CH_4. Vacuum 48(10):817–824

Bentz JA, Tompson RV, Loyalka SK (2001) Measurements of viscosity, velocity slip coefficients, and tangential momentum accommodation coefficients using a modified spinning rotor gauge. J Vac Sci Technol A Vac Surf Films 19(1):317–324

Beskok A, Karniadakis GE (1994) Simulation of heat and momentum transfer in complex micro-geometries. J Thermophys Heat Transf 8(4):647–655

Bidkar RA, Tung RC, Alexeenko AA, Sumali H, Raman A (2009) Unified theory of gas damping of flexible microcantilevers at low ambient pressures. Appl Phys Lett. doi:10.1063/1.3122933

Cao BY, Chen M, Guo ZY (2005) Temperature dependence of the tangential momentum accommodation coefficient for gases. Appl Phys Lett. doi:10.1063/1.1871363

Chirita V, Pailthorpe BA, Collins RE (1993) Molecular dynamics study of low-energy Ar scattering by the Ni(001) surface. J Phys D Appl Phys 26(1):133–142

Chirita V, Pailthorpe BA, Collins RE (1997) Non-equilibrium energy and momentum accommodation coefficients of Ar atoms scattered from Ni(0 0 1) in the thermal regime: a molecular dynamics study. Nucl Instrum Methods Phys Res B Beam Interact Mater Atoms 129(4):465–473

Clelanda AN, Aldridge JS, Driscoll DC, Gossard AC (2002) Nanomechanical displacement sensing using a quantum point contact. Appl Phys Lett 81:1699–1701

Ekinci KL, Roukes ML (2008) Nanoelectromechanical systems. Rev Sci Instrum. doi:10.1063/1.1927327

Enguang D (2002) Surface-related phase noise in SAW resonators. IEEE Trans Ultrason Ferroelectr Freq Control 49:649–655

Evans DJ, Hoover WG (1986) Flows far from equilibrium via molecular-dynamics. Annu Rev Fluid Mech 18:243–264

Feng C, Jiang LY (2011) Molecular dynamics simulation of squeeze-film damping effect on nano resonators in the free molecular regime. Phys E 43:1605–1609

Finger GW, Kapat JS, Bhattacharya A (2007) Molecular dynamics simulation of adsorbent layer effect on tangential momentum accommodation coefficient. J Fluids Eng Trans ASME. doi:10.1115/1.2375128

Fukui S, Shimada H, Yamane K, Matsuoka H (2005) Flying characteristics in the free molecular region (influence of accommodation coefficients). Microsyst Technol. doi:10.1007/s00542-005-0538-0

Gad-el-Hak M (1999) The fluid mechanics of microdevices—the Freeman Scholar Lecture. J Fluids Eng Trans ASME 121:5–33

Gallis MA, Torczynski JR (2004) An improved Reynolds-equation model for gas damping of microbeam motion. J Microelectromech Syst 13(4):653–659

Goodman FO, Wachman HY (1976) Dynamics of gas–surface scattering. Academic Press, New York

Gronych T, Ulman R, Peksa L, Repa P (2004) Measurements of the relative momentum accommodation coefficient for different gases with a viscosity vacuum gauge. Vacuum 73(2):275–279

Guo X, Alexeenko A (2009) Compact model of squeeze-film damping based on rarefied flow simulations. J Micromech Microeng. doi:10.1088/0960-1317/19/4/045026

Honig CDF, Sader JE, Mulvaney P, Ducker WA (2010) Lubrication forces in air and accommodation coefficient measured by a thermal damping method using an atomic force microscope. Phys Rev E. doi:10.1103/PhysRevE.81.056305

Huang B, Li Z, Liu Z, Zhou G, Hao S, Wu J, Gu BL, Duan W (2008) Adsorption of gas molecules on graphene nanoribbons and its implication for nanoscale molecule sensor. J Phys Chem C 112:13442–13446

Husain A, Hone J, Postma HWC, Huang XMH, Drake T, Barbic M, Scherer A, Roukesa ML (2003) Nanowire-based very-high-frequency electromechanical resonator. Appl Phys Lett 83:1240–1242

Irving JH, Kirkwood JG (1950) The statistical mechanical theory of transport processes. IV. The equations of hydrodynamics. J Chem Phys 18:817–829

Karniadakis GE, Beskok A, Aluru N (2005) Micro flows and nano flows: fundamentals and simulation. Springer, New York

Lee J, Aluru NR (2010) Separation of gases from gas–water mixtures using carbon nanotubes. Appl Phys Lett 96:133108

Rettner CT (1998) Thermal and tangential-momentum accommodation coefficients for N2 colliding with surfaces of relevance to disk-drive air bearings derived from molecular beam scattering. IEEE Trans Magn 34(4):2387–2395

Sazhin OV, Borisov SF, Sharipov F (2001) Accommodation coefficient of tangential momentum on atomically clean and contaminated surfaces. J Vac Sci Technol A Vac Surf Films 19(5):2499–2503

Sone Y, Takata S, Ohwada T (1990) Numerical analysis of the plane Couette flow of a rarefied gas on the basis of the linearized Boltzmann equation for hard sphere molecules. Eur J Mech B Fluids 9:273–288

Sun J, Li ZX (2008) Effect of gas adsorption on momentum accommodation coefficients in microgas flows using molecular dynamic simulations. Mol Phys 106:2325–2332

Sun J, Li ZX (2010) Two-dimensional molecular dynamic simulations on accommodation coefficients in nanochannels with various wall configurations. Comput Fluids. doi:10.1016/j.compfluid.2010.04.004

Sun J, Li ZX (2011) Three-dimensional molecular dynamic study on accommodation coefficients in rough nanochannels. Heat Transfer Eng. doi:10.1080/01457632.2010.509759

Todd BD, Evans DJ, Daivis PJ (1995) Pressure tensor for inhomogeneous fluids. Phys Rev E. doi:10.1103/PhysRevE.52.1627

Veijola T, Kuisma H, Lahdenperi J (1998) The influence of gas-surface interaction on gas-film damping in a silicon accelerometer. Sensors Actuators A 66:83–92

Verbridge SS, Craighead HG, Parpia JM (2008) A megahertz nanomechanical resonator with room temperature quality factor over a million. Appl Phys Lett. doi:10.1063/1.2822406

Yamamato K, Takeuchi H, Hyakutake T (2006) Characteristics of reflected gas molecules at a solid surface. Phys Fluids. doi:10.1063/1.2191871

Yang YT, Callegari C, Feng XL, Roukes ML (2011) Surface adsorbate fluctuations and noise in nanoelectromechanical systems. Nano Lett 11:1753–1759

Zhang WM, Meng G, Zhou JB, Chen JY (2009) Nonlinear dynamics and chaos of microcantilever-based TM-AFMs with squeeze film damping effects. Sensors. doi:10.3390/s90503854

Zhou L (2007) Adsorption: progress in fundamental and application research. World Scientific, New York